*Int. J. Heat Mass Transfer.* Vol. 30, No. 9, pp. 1907–1925, 1987
Printed in Great Britain

0017–9310/87 $3.00 + 0.00
Pergamon Journals Ltd.

# An evaluation of eleven discretization schemes for predicting elliptic flow and heat transfer in supersonic jets†

M. PATEL, M. CROSS and N. C. MARKATOS
Centre for Numerical Modelling and Process Analysis, Thames Polytechnic, London SE18 6PF, U.K.

and

A. C. H. MACE
RARDE, Fort Halstead, Sevenoaks, Kent, U.K.

(*Received* 30 *July* 1986 *and in final form* 21 *January* 1987)

**Abstract**—The paper describes studies to quantify the numerical errors caused by 'false diffusion', and to compare the performance of alternative numerical schemes for describing elliptic convective flow and heat transfer, within supersonic jets mixing into supersonic or subsonic streams. Results obtained are presented and discussed. Eleven schemes were considered in this study, but converged solutions were obtained with only five of them. Results obtained with the successful schemes are presented and discussed. It is concluded that for the high-shearing, high-velocity flows considered, the 'upwind' differencing scheme is probably the best choice, despite its dissipative nature and that the numerical errors associated with its use are no more significant than those introduced by uncertainties in the turbulence models.

## 1. INTRODUCTION

TECHNIQUES for calculating the hydrodynamics and heat transfer of supersonic jets exhausting into supersonic or subsonic streams have been reported in ref. [1]. The case of interest here is when the radius of a wall surrounding the jet nozzle is significantly larger than the nozzle exit radius. In these circumstances recirculating flow next to the thick wall necessitates the solution of elliptic differential equations. A solution procedure for predicting such flows has been reported in ref. [1], where finite-volume equations are formulated using upwind differencing. A study of the predictions obtained by this procedure has suggested that the profiles of variables may be 'smeared' [2]. Although 'smearing' may be due to physical interactions, it may also be attributed to artificial diffusion introduced by the upwind differencing scheme. In the present work 'false-diffusion' introduced by the upwind scheme is quantified, in relation to the real physical diffusion. Furthermore, alternative schemes [3–17] that claim to introduce less 'false diffusion' have been implemented in a computer program, and used to obtain predictions that are compared among themselves. Predictions using different turbulence-model constants were also obtained in order to compare the magnitude of 'false-diffusion' error with the error introduced by the physical uncertainty in the turbulence modelling.

For computational efficiency, calculations have been performed for chemically inert flows. The underlying conclusions are not expected to be materially different in nature for chemically reacting conditions.

## 2. THE PHYSICAL PROBLEM CONSIDERED

The physical problem considered in this study is similar to that reported in ref. [1], and it is shown in Fig. 1. It concerns a hot supersonic jet exhausting into a cold subsonic freestream.

The freestream and jet stream separate from the wall at A and B, respectively, transferring momentum to the fluid in the trapped region by turbulent mixing. To preserve continuity, the flow dividing lines AC and BC meet at C, a stagnation point. The trapped gases

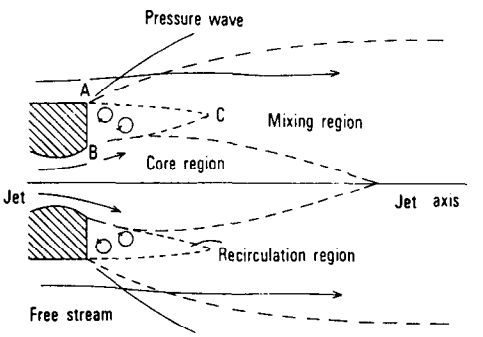


FIG. 1. Flowfield around the nozzle exit.

## NOMENCLATURE

| | |
|---|---|
| $A_i$ | influence coefficients ($i$ = N, S, E, W) |
| $a_i$ | cell face area |
| $C_i$ | convective contribution in false diffusion approximation |
| $C_p$ | specific heat |
| $D_i$ | diffusion contribution in false diffusion approximation |
| $F_{xe}$ | weighting function |
| $h$ | enthalpy |
| $k$ | turbulent kinetic energy |
| $M$ | freestream Mach number |
| $m_i$ | mass flow rate across cell face $i$ |
| $M^+$ | coefficient |
| $p$ | pressure |
| $p_\infty$ | freestream pressure |
| $P$ | Peclet number |
| $P_i$ | grid Peclet number across cell face $i$ |
| $S_\phi$ | source term in transport equation |
| $S_U^\phi$, $S_P^\phi$ | linearized coefficients in the source term |
| $T$ | temperature |
| $u$ | component of velocity |
| $v$ | component of velocity. |

Greek symbols

| | |
|---|---|
| $\beta_e$ | weighting factor |
| $\delta_i$ | distance between node P and $i$ (= N, S, E, W) |
| $\varepsilon$ | dissipation rate of turbulence energy |
| $\phi$ | transported variable |
| $\rho$ | density of fluid |
| $\mu$ | viscosity |
| $\Gamma$ | diffusion exchange coefficient |
| $\theta$ | angle of flow into a cell. |

circulate as a pair of vortices and an increase in pressure at C preserves this circulating motion. The nature of the flow pattern in the region ABC will depend upon the magnitude of the nozzle and freestream velocities. For the computations reported here the nozzle exit plane and freestream conditions used are listed in Table 1. The ratio of the wall diameter to the nozzle exit diameter is 4, and a recirculation region exists close to the wall. All variables across the nozzle and freestream inlet are set uniformly to those of the jet and ambient conditions, respectively.

The jet and freestream inlet values of turbulence kinetic energy ($k$) and its dissipation rate ($\varepsilon$) are defined for the present calculations as

$$k_{\text{inlet}} = 0.005 u_{\text{inlet}}^2 \tag{1}$$

and

$$\varepsilon_{\text{inlet}} = C_D k_{\text{inlet}}^{3/2} / 0.1 r_{\text{nozzle}} \tag{2}$$

where $C_\mu = 0.09$ and $r_{\text{nozzle}}$ is the nozzle radius.

Table 1. Conditions at the inlet of the calculation domain

| Variable $\phi$ | Nozzle stream values | Freestream values |
|---|---|---|
| Axial velocity, m s$^{-1}$ | 2000.0 | 200.0 |
| Radial velocity, m s$^{-1}$ | 0.0 | 0.0 |
| Pressure, kPa | 200.0 | 100.0 |
| Temperature, K | 900.0 | 217.0 |
| Mach number | 3.3 | 0.68 |
| Density, kg m$^{-3}$ | 0.77 | 1.6 |
| Radius of nozzle exit, m | 0.1 | — |
| Radius of wall, m | 0.4 | — |

Note: All variables are set uniformly across the nozzle exit plane and freestream inlet boundary.

## 3. THE MATHEMATICAL MODEL

### 3.1. *The differential equations*

The partial differential equations describing the fluid dynamics and heat transfer of the flow problem described above are written in the following time-averaged, two-dimensional form, with axial and radial coordinates $x$ and $r$, respectively [1]:

$$\frac{\partial}{\partial x}(\rho u \phi) + \frac{1}{r}\frac{\partial}{\partial r}(r \rho v \phi) - \frac{\partial}{\partial x}\left(\frac{\mu}{\sigma_\phi}\frac{\partial \phi}{\partial x}\right) - \frac{1}{r}\frac{\partial}{\partial r}\left(\frac{r\mu}{\sigma_\phi}\frac{\partial \phi}{\partial r}\right) = S_\phi. \tag{3}$$

This represents a transport equation for a general variable $\phi$. The variables $u$ and $v$ are axial and radial velocity components, $\rho$ is the density, $\mu$ the effective viscosity and $\sigma_\phi$ the ratio of the rate of exchange of $\phi$ to the rate of exchange of momentum. The final term, $S_\phi$, is the source term. The variables, $\phi$, necessary in this study are: $u$, $v$, $h$, $k$ and $\varepsilon$, where $h$ is the total enthalpy, expressed as

$$h = C_p T + \frac{u^2 + v^2}{2} + k \tag{4}$$

and $C_p$ is the specific heat. $k$ and $\varepsilon$ stand for the kinetic energy of turbulence and its dissipation rate.

Source-term expressions for the above $\phi$'s are given in ref. [1]. Pressure is derived from the pressure correction equation [18].

Further relationships are required for: the density of the gas, from the ideal gas equation; the pressure, derived by applying the continuity condition to all local fluid volumes; and the temperature, obtained from the enthalpy definition.

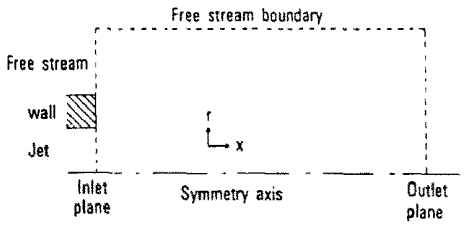


FIG. 2. The solution domain.

### 3.2. *The boundary conditions*

The boundary conditions relate to the solution domain of Fig. 2. This extends axially from an inlet plane coplanar with the jet exit, to an outlet plane downstream from the recirculation region. The radial extent is from the symmetry axis to an outer location beyond the wall radius and sufficient to enclose the expanding jet.

With $\phi(x, r)$ referring to any variable at position $(x, r)$, and $\phi_\infty = \phi\ (0, r > r_{\text{wall}})$, the boundary conditions are as follows:

(i) Symmetry axis, $r = 0$; $v = 0$, $\partial\phi/\partial r = 0$.

(ii) Outer boundary, $r = r_{\text{outer}}$; $\phi = \phi_\infty$, except $v$; subsonic freestream, $v = 0$; supersonic freestream, $v = v_\infty + [(p - p_\infty)/\rho_\infty u](M^2 - 1)^{1/2}$, where $M$ is the freestream Mach number at the inlet plane [1].

(iii) The outlet boundary, $x = x_{\text{outlet}}$; $\partial\phi/\partial x = 0$, except for subsonic freestream pressure, $p = p_\infty$.

(iv) The inlet boundary, $x = 0$; $r \geqslant r_{\text{wall}}$, $\phi = \phi_\infty$; $r \leqslant r_{\text{nozzle}}$, $\phi = \phi_{\text{jet}}$; $r_{\text{wall}} > r > r_{\text{nozzle}}$, $u = 0$; $v$, $k$, and $\varepsilon$ are defined using logarithmic wall functions [18].

## 4. METHOD OF SOLUTION

### 4.1. *Finite-domain equations*

Equation (3) may be written in finite-volume form by multiplying by $r$ and integrating over an elemental cell volume surrounding a defined point P [3, 18]

$$\sum_n (A_n^\phi - S_P^\phi)\phi_P = \sum_n A_n^\phi \phi_n + S_U^\phi \tag{5}$$

where the summation $n$ is over the cells adjacent to P. The coefficients $A_n^\phi$ account for convective and diffusive fluxes across an elemental cell. For example, when upwind differencing is used, the coefficient for the high-$x$ neighbour is

$$\left.\begin{aligned} A_n^\phi &= \left(\frac{\mu}{\sigma_\phi}\right)\frac{a_n}{\delta_n} \quad \text{when} \quad u_n < 0 \\ \text{and} \\ A_n^\phi &= \rho_P u_n a_n + \left(\frac{\mu}{\sigma_\phi}\right)_n \frac{a_n}{\delta_n} \quad \text{when} \quad u_n \geqslant 0 \end{aligned}\right\} \tag{6}$$

where $\delta_n$ is the distance between nodes P and $n$, $a_n$ is the area of the cell face, $(\mu/\sigma_\phi)_n$ is the arithmetic mean of the values at P and $n$, and $\rho_P$ is the upwind value of density (in this case that at grid node P). The source term is written in a linear form, $S_\phi = S_U^\phi + S_P^\phi \phi_P$.

This formulation of the above coefficients, and in particular of their convection part, constitutes the essence of this study.

### 4.2. *Problems associated with the coefficient formulation*

The discretization procedure briefly described in the previous section involves use of interpolation assumptions for the variations of the fluid properties. In principle, interpolation assumptions will not affect final solutions, provided sufficiently fine grids are employed. They will affect solutions when coarse grids are used; this is particularly the case for the interpolation of convection terms. For multi-dimensional, multi-phase flow phenomena, involving two and three space dimensions and two or more sets of equations, the power of even present day computer capacity and speed generally proves to be the limiting factor in the use of very fine grids. Therefore, interpolation schemes for the convection terms, that are sufficiently accurate to permit the performance of complex calculations within presently available computing resources, are required. One of the main deficiencies of current interpolation assumptions relates to the so-called 'false diffusion', commonly attributed in the literature to the order of accuracy of the differencing scheme used. Whilst the order of the scheme may be a component of the problem it cannot be the only contributor. Because, for high Peclet number flows, even though the central difference scheme is second-order accurate it actually performs far less satisfactory than the upwind scheme which is only first-order accurate [3]. Indeed, the performance of the upwind scheme is also unsatisfactory, for it smears profiles at large Peclet numbers, a feature which is true of all other 'higher order' schemes, in different degrees [23]. The view taken in this report is that asserted by Patankar [3]: false diffusion exists only in multi-dimensional phenomena and arises primarily because of the common practice of treating the flow across each control-cell face as locally one-dimensional. Therefore, schemes that would give less false diffusion should take account of the local multi-dimensional nature of the flow. Such schemes exist but they present convergence problems [10, 11]. The true merit of the higher-order schemes is that they approximate better the fluid property–space variation which is in reality nonlinear; so they may be more accurate for relatively coarse grids. In this work eleven alternative schemes are tested with a view to evaluating their relative accuracy, generality, numerical stability and computer requirements.

The schemes tested are:

(1) the central-difference scheme (CDS);
(2) the upwind-difference scheme (UDS);
(3) the hybrid-difference scheme (HDS);
(4) the locally-exact-difference scheme (LEDS);
(5) the power-difference scheme (PDS);
(6) the quadratic upstream-difference scheme [8] (QUDS);

(7) the extended quadratic upstream-difference scheme [9] (QUDSE);

(8) the extended/revised quadratic upstream-difference scheme [9] (QUDSER);

(9) the skew scheme [10, 11] (SKEW);

(10) the residual-difference scheme [16] (RDS); and finally

(11) the upwind-in-streamline-direction [17] scheme (UPSTREAM).

These schemes are described in detail in the next section.

### 4.3. *Coefficient formulation according to the various schemes*

4.3.1. *The diffusion term.* Integration of the differential equation diffusion terms (3) over a typical control volume, P (Fig. 3) yields

$$\int_{x_w}^{x_e}\int_{r_s}^{r_n} -\left\{\frac{\partial}{\partial x}\left(\frac{\mu}{\sigma_\phi}\frac{\partial\phi}{\partial x}\right)+\frac{1}{r}\frac{\partial}{\partial r}\left(\frac{r_\mu}{\sigma_\phi}\frac{\partial\phi}{\partial r}\right)\right\}$$

$$=\left(\frac{\mu}{\sigma_\phi}\frac{\partial\phi}{\partial x}\right)_e a_e-\left(\frac{\mu}{\sigma_\phi}\frac{\partial\phi}{\partial x}\right)_w a_w+\left(\frac{\mu}{\sigma_\phi}\frac{\partial\phi}{\partial r}\right)_n a_n-\left(\frac{\mu}{\sigma_\phi}\frac{\partial\phi}{\partial r}\right)_s a_s. \tag{7}$$

Approximations for the quantities in brackets are sought and the standard practice is to use central differencing. The right-hand side of equation (7) then becomes

$$\left(\frac{\mu}{\sigma_\phi}\right)_e\frac{a_e}{\delta_e}(\phi_E-\phi_P)-\left(\frac{\mu}{\sigma_\phi}\right)_w\frac{a_w}{\delta_w}(\phi_W-\phi_P)$$

$$+\left(\frac{\mu}{\sigma_\phi}\right)_n\frac{a_n}{\delta_n}(\phi_N-\phi_P)-\left(\frac{\mu}{\sigma_\phi}\right)_s\frac{a_s}{\delta_s}(\phi_S-\phi_P) \tag{8}$$

where $\delta_i$ is the distance between nodes P and $i$. This approximation is third order [8].

4.3.2. *The convection term.* Integration of the convection terms of equation (3) over a typical control volume P (Fig. 3) yields

$$\int_{x_w}^{x_e}\int_{r_s}^{r_n}\left\{\frac{1}{r}\frac{\partial}{\partial r}(r\rho v\phi)+\frac{\partial}{\partial x}(\rho u\phi)\right\}$$

$$=(\rho u\phi)_e a_e-(\rho u\phi)_w a_w+(\rho v\phi)_n a_n-(\rho v\phi)_s a_n. \tag{9}$$

The various $\phi$-value approximations used at the control-volume faces are given below.

(1) *Central-difference scheme*

The central-difference scheme assumes a linear profile to evaluate the convected face values as follows:

$$\phi_e=\tfrac{1}{2}(\phi_E+\phi_P)$$
$$\phi_w=\tfrac{1}{2}(\phi_W+\phi_P),\ \text{etc.} \tag{10}$$

Then, for the central-difference scheme one can express the influence coefficients of equation (5) (e.g. $A_n$, containing contributions of both convection and diffusion) as follows:

$$A_E=D_e-\text{mod}\left\{\frac{C_e}{2}\right\}+[\![-C_e,0]\!]$$

$$A_W=D_w-\text{mod}\left\{\frac{C_w}{2}\right\}+[\![C_w,0]\!]$$

$$A_N=D_n-\text{mod}\left\{\frac{C_n}{2}\right\}+[\![-C_n,0]\!]$$

$$A_S=D_s-\text{mod}\left\{\frac{C_s}{2}\right\}+[\![C_s,0]\!] \tag{11}$$

where the diffusion terms $D_i$ are

$$D_i=\left(\frac{\mu}{\sigma_\phi}\right)\frac{a_i}{\delta_i} \tag{12}$$

the convection terms $C_i$ are

$$C_i=\rho_i u_i a_i \tag{13}$$

and

$$[\![A,B]\!]\equiv\max(A\text{ and }B).$$

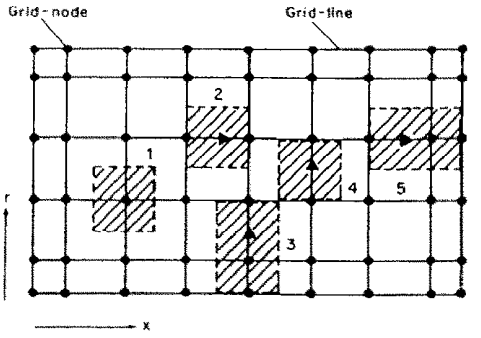


| Number | 1 | 2 | 3 | 4 | 5 |
|---|---|---|---|---|---|
| Control volume type | $\phi$ and continuity | U | V boundary | V | U boundary |

CONTROL VOLUME SPECIFICATION

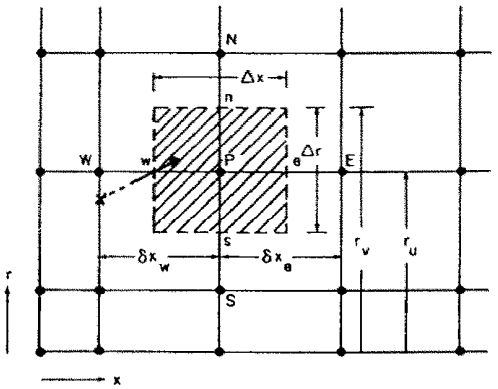


CONTROL VOLUME FOR SCALAR VARIABLE

FIG. 3. Control volume and notation.

This is a convenient way of presenting the various schemes and will be used for them all.

(2) *Upwind-difference scheme*

The upwind-difference scheme, first suggested by Courant *et al.* [5] assumes the upwind $\phi$-value to be convected through the faces, instead of the average of two neighbouring values of the convected property. This leads to the following approximation for the convected $\phi$-values at the faces:

$$\begin{aligned}
\phi_e &= \phi_P \quad U_e \geqslant 0 \\
&= \phi_E \quad U_e < 0 \\
\phi_w &= \phi_W \quad U_w \geqslant 0 \\
&= \phi_P \quad U_w < 0 \\
\phi_n &= \phi_P \quad V_n \geqslant 0 \\
&= \phi_N \quad V_n < 0 \\
\phi_s &= \phi_S \quad V_s \geqslant 0 \\
&= \phi_P \quad V_s < 0.
\end{aligned} \tag{14}$$

The influence coefficients for the upwind-difference scheme are

$$\begin{aligned}
A_E &= [\![D_e, D_e - C_e]\!] \\
A_W &= [\![D_w, D_w + C_w]\!] \\
A_N &= [\![D_n, D_n - C_n]\!] \\
A_S &= [\![D_s, D_s + C_s]\!]
\end{aligned} \tag{15}$$

using the previously defined notation.

(3) *Hybrid-difference scheme*

The hybrid-difference scheme, introduced by Spalding [6] combines the advantages of both the central-difference scheme and the upwind-difference scheme. It leads to the following expressions for the convected face values:

$$\begin{aligned}
\phi_e &= \phi_P \quad \dot{m}_e > 2D_e \\
&= \tfrac{1}{2}(\phi_P + \phi_E) \quad \dot{m}_e \leqslant 2D_e \\
\phi_w &= \phi_W \quad \dot{m}_w > 2D_w \\
&= \tfrac{1}{2}(\phi_P + \phi_W) \quad \dot{m}_w \leqslant 2D_w \\
\phi_n &= \phi_P \quad \dot{m}_n > 2D_n \\
&= \tfrac{1}{2}(\phi_P + \phi_N) \quad \dot{m}_n \leqslant 2D_n \\
\phi_s &= \phi_S \quad \dot{m}_s > 2D_s \\
&= \tfrac{1}{2}(\phi_P + \phi_S) \quad \dot{m}_s \leqslant 2D_s
\end{aligned} \tag{16}$$

where $\dot{m}$'s are the absolute values of the mass-flow rates through each face denoted by the lower-case subscripts.

The influence coefficients for the hybrid-difference scheme are

$$\begin{aligned}
A_E &= [\![0, D_e, -C_e/2, -C_e]\!] \\
A_W &= [\![0, D_w, C_w/2, C_w]\!] \\
A_N &= [\![0, D_n, -C_n/2, -C_n]\!] \\
A_S &= [\![0, D_s, C_s/2, C_s]\!].
\end{aligned} \tag{17}$$

(4) *Locally-exact-difference scheme*

The locally-exact-difference scheme, traced back to the paper by Allen and Southwell [4] and later rediscovered by Spalding [6] and others, makes use of the one-dimensional analytical solution for the convection–diffusion equation (without sources) to approximate the convected values across the faces.

Since the analytical solution for the one-dimensional convection–diffusion equation is an exponential function, the face values according to this scheme are approximated as follows:

$$\begin{aligned}
\phi_w &= \phi_W + \frac{\exp(P_w) - 1}{\exp(P) - 1}(\phi_P - \phi_W) \\
\phi_e &= \phi_P + \frac{\exp(P_e) - 1}{\exp(P) - 1}(\phi_E - \phi_P) \\
\phi_n &= \phi_P + \frac{\exp(P_n) - 1}{\exp(P) - 1}(\phi_N - \phi_P) \\
\phi_s &= \phi_S + \frac{\exp(P_s) - 1}{\exp(P) - 1}(\phi_P - \phi_S)
\end{aligned} \tag{18}$$

where $P$ is the Peclet number and $P_e$, $P_w$, etc. are the mesh Peclet numbers (e.g. $P_n = C_n/D_n = \rho_n u_n(\sigma_\phi/\mu)$).

The influence coefficients for the locally-exact-difference scheme are

$$\begin{aligned}
A_E &= \frac{P_e}{\exp(P_e) - 1} + [\![-C_e, 0]\!] \\
A_W &= \frac{P_w}{\exp(P_w) - 1} + [\![C_w, 0]\!] \\
A_N &= \frac{P_n}{\exp(P_n) - 1} + [\![-C_n, 0]\!] \\
A_S &= \frac{P_s}{\exp(P_s) - 1} + [\![C_s, 0]\!].
\end{aligned} \tag{19}$$

(5) *Power-difference scheme*

The power-difference scheme, an extension of the locally-exact-difference scheme, makes use of a fifth-order power law to approximate the exponential functions of the locally-exact-difference scheme [3]. The convected value at the faces is approximated as follows:

$$(1 + \beta_e)\phi_{\text{upstream}} - \beta_e \phi_{\text{downstream}} \tag{20}$$

where

$$\beta_e = (1 - |P_e|/10)^5/|P_e|. \tag{21}$$

The influence coefficients for the power-difference

scheme are:

$$A_E = D_e[\![0, \beta_e|P_e|]\!] + [\![-C_e, 0]\!]$$
$$A_W = D_w[\![0, \beta_w|P_w|]\!] + [\![C_w, 0]\!]$$
$$A_N = D_n[\![0, \beta_n|P_n|]\!] + [\![-C_n, 0]\!]$$
$$A_S = D_s[\![0, \beta_s|P_s|]\!] + [\![C_s, 0]\!]. \quad (22)$$

(6) *Quadratic upstream-difference scheme*

The quadratic upstream-difference scheme, proposed by Leonard [8] is claimed to combine the accuracy of quadratic interpolation with the stability of upstream weighting. This scheme can be interpreted as a pure upwind scheme which is, however, augmented by gradient/curvature-type correction terms. This allows, the $\phi_w$-value, for example, to respond to the transport processes which occur only in directions normal to that considered. In other words, it allows the coupling of the component flows through one-dimensional approximations which, however, include corner nodes when the curvature-type corrections are made. According to this scheme, the $\phi$-values being convected through the control-volume faces are expressed, as follows:

$$\phi_e = \frac{1}{2}(\phi_P + \phi_E) - \frac{1}{8}\left\{\frac{U_e + |U_e|}{2U_e}(\phi_E + \phi_W - 2\phi_P) + \frac{U_e - |U_e|}{2U_e}(\phi_P + \phi_{EE} - 2\phi_E)\right\}$$

$$\phi_w = \frac{1}{2}(\phi_P + \phi_W) - \frac{1}{8}\left\{\frac{U_w + |U_w|}{2U_w}(\phi_P + \phi_{WW} - 2\phi_W) + \frac{U_w + |U_w|}{2U_w}(\phi_W + \phi_E - 2\phi_P)\right\}. \quad (23)$$

The influence coefficients are

$$A_E = M_e^+(D_e - 3C_e/8) + M_e^-(D_e - 3C_e/4 - C_w/8)$$
$$A_W = M_w^-(D_w + 3C_w/8) + M_w^+(D_w - 3C_w/4 + C_e/8)$$
$$A_N = M_n^+(D_n - 3C_n/8) + M_n^-(D_n - 3C_n/4 - C_s/8)$$
$$A_S = M_s^-(D_s + 3C_s/8) + M_s^+(D_s + 3C_s/4 + C_n/8)$$
$$S_a^{QUDS} = S_a^{UDS} - (M_w^+ C_w \phi_{WW} + M_s^+ C_s \phi_{SS} - M_e^- C_e \phi_{EE} - M_n^- C_n \phi_{NN})$$
$$S_b^{QUDS} = S_b^{UDS} + (M_e^+ C_e + M_n^+ C_n - M_w^- C_w - M_s^- C_s)/8 \quad (24)$$

where

$$M_j^{\pm} = (C_j \pm |C_j|)/(2C_j), \quad j = e, w, n, s$$

and $S_a^{UDS}$, $S_b^{UDS}$ are the conventional UDS sources.

(7) *Quadratic upstream-difference scheme extended*

The quadratic upstream-difference scheme extended, reported by Pollard and Siu [9], is an extension of the quadratic upstream-difference scheme, in that the influence coefficients are re-formulated to ensure positive coefficients. For example, when the flow is from left to right and bottom to top, then the quadratic upstream coefficients, neglecting diffusion are

$$A'_E = \{\tfrac{3}{8}C_e\} \qquad A'_N = \{\tfrac{3}{8}C_n\}$$
$$A'_W = -\{\tfrac{1}{8}C_e + \tfrac{3}{4}C_w\} \qquad A'_S = \{\tfrac{1}{8}C_n + \tfrac{3}{4}C_s\}$$
$$A_{WW} = \{\tfrac{1}{8}C_w\} \qquad A_{SS} = \{\tfrac{1}{8}C_s\} \quad (25)$$

which are replaced in the quadratic upstream difference scheme extended by

$$A'_E = \{\tfrac{3}{4}C_e\} \qquad A'_N = \{\tfrac{3}{4}C_n\}$$
$$A'_W = \{\tfrac{3}{4}C_w + \tfrac{1}{8}C_e\} \qquad A'_S = \{\tfrac{3}{4}C_s + \tfrac{1}{8}C_n\}$$
$$A_{WW} = 0 \qquad A_{SS} = 0$$
$$S_a = -\tfrac{1}{8}[C_w\phi_{WW} + C_s\phi_{SS}] - \tfrac{9}{8}(C_e\phi_E + C_n\phi_N)$$
$$S_b = -\tfrac{1}{8}[C_e + C_n] - \tfrac{9}{8}(C_w + C_n) \quad (26)$$

where primes (′) denote without diffusion.

(8) *Revised/extended upstream-difference scheme*

The extended/revised version of the quadratic upstream-difference scheme requires a further modification of the source term, namely, its linearization.

(9) *SKEW-difference scheme*

The SKEW-difference scheme is a form of flow-oriented differencing and was reported by Raithby [10, 11]. It aims to reduce or even eliminate 'false diffusion', an inherent problem of locally one-dimensional schemes. The earliest reported flow-oriented scheme is believed to be the one reported by Le Feuvre [12] and independently by Zuber [13]. However, these were non-conservative, and their use was rather limited.

The Raithby skew scheme uses four distinct interpolation regions (to account for all possibilities of flow direction) to evaluate the convected $\phi$-value at the east face of the control volume. These are represented in Fig. 3. The approximation for $\phi_e$ for the particular inclination of Fig. 3 is

$$(\rho u)_e \Delta y \phi_e = (\tfrac{1}{2}C_e - K_e)2\phi_P + 2K_e\phi_S \quad (27)$$

where

$$K_e = \left|\frac{C_e}{2}\right|_{min}\left[1, \frac{1}{2}\left|\frac{U_e}{V_e}\right|\frac{\delta x}{\delta y}\right] = \frac{1}{2}C_{emin}\left[1, \frac{1}{2}\tan\theta_e\frac{\delta x}{\delta y}\right]. \quad (28)$$

Similar expressions can be obtained for all other possibilities. The weighting factor used, for example

$$F_{xe} = \frac{1}{2}\left|\frac{U_e}{V_e}\right|\frac{\delta x}{\delta y} \quad (29)$$

has to be restricted to be less than unity to avoid extrapolations, i.e. in Raithby's skew scheme it is restricted between zero and one. However, interpolation is used for weighting functions greater than unity [12]. For $F_{xe}$ equal to zero, there is no cross-

stream velocity component and the skew scheme reduced to the conventional upwind-difference scheme.

In essence, the skew scheme, accounts for grid-to-flow skewness (i.e. the main cause of false diffusion), but at the expense of stability and conservation.

The influence coefficients for the skew-difference scheme are

$$\begin{aligned} A_{\mathrm{E}} &= D_e-(C_e/2-K_e)(1-S_{ue}) \\ A_{\mathrm{W}} &= D_w+(C_w/2-K_w)(1+S_{uw}) \\ A_{\mathrm{N}} &= D_n-(C_n/2-K_n)(1-S_{un}) \\ A_{\mathrm{S}} &= D_s+(C_s/2-K_s)(1+S_{vs}) \end{aligned} \tag{30}$$

where the $S$'s take the sign of the subscripted velocity components and the SE, SW, NE, NW contributions are included in the source term after linearization. For a full formulation see Patel [15].

(10) *Residual-difference scheme*

The residual-difference scheme [14] is obtained by considering the residual for each coordinate direction. The complete equation yields approximations which depend on the mesh Peclet numbers and exponential functions. For illustration purposes, consider the one-dimensional equation (with sources) evaluated with guessed values of the $\phi$ variable. This leads to

$$\rho u\frac{\mathrm{d}\phi}{\mathrm{d}x}-\Gamma\frac{\mathrm{d}^2\phi}{\mathrm{d}x^2}-S_\phi=\mathrm{Res} \tag{31}$$

whereby substitution of the form

$$\phi=A_0+A_1x+A_2\exp(\rho ux/\Gamma) \tag{32}$$

leads to

$$\frac{\rho u}{2\Delta x}(\phi_{\mathrm{E}}-\phi_{\mathrm{W}})-\frac{\Gamma}{\Delta x}Q[Px](\phi_{\mathrm{E}}+\phi_{\mathrm{W}}-2\phi_{\mathrm{P}}) -S_\phi=\mathrm{Res} \tag{33}$$

where

$$\begin{aligned} Px &= \frac{\rho u}{\Gamma}\Delta x, \quad Q[Px]=1+Px^2/16, \quad \text{for } |Px|<4 \\ &= \frac{|Px|}{2}, \qquad\qquad \text{for } |Px|\geqslant 4 \end{aligned} \tag{34}$$

and the finite-difference scheme is obtained by setting Res, the residual, to zero.

The influence coefficients for the residual-difference scheme are

$$\begin{aligned} A_{\mathrm{E}} &= D_eQ[\![P_e]\!]-\mathrm{mod}\left\{\frac{C_e}{2}\right\}+[\![-C_e,0]\!] \\ A_{\mathrm{W}} &= D_wQ[P_w]-\mathrm{mod}\left\{\frac{C_w}{2}\right\}+[\![C_w,0]\!] \\ A_{\mathrm{N}} &= D_nQ[P_n]-\mathrm{mod}\left\{\frac{C_n}{2}\right\}+[\![-C_n,0]\!] \\ A_{\mathrm{S}} &= D_sQ[P_s]-\mathrm{mod}\left\{\frac{C_s}{2}\right\}+[\![C_s,0]\!] \end{aligned} \tag{35}$$

where $Q[P]$ is given by equation (34).

(11) *UPSTREAM scheme (modified)*

The coefficients of the finite-domain equations are formulated as follows, where attention is focused, e.g. at the SW corner of the control cell:

$$\left.\begin{aligned} C_w\phi_w &= C_wA\phi_{\mathrm{W}}+C_wB\phi_{\mathrm{SW}} \\ C_s\phi_s &= C_s\phi_{\mathrm{W}} \end{aligned}\right\} \quad \theta_2<45$$

$$\left.\begin{aligned} C_s\phi_s &= C_sA\phi_{\mathrm{S}}-C_sB\phi_{\mathrm{SW}} \\ C_w\phi_w &= C_w\phi_{\mathrm{W}} \end{aligned}\right\} \quad \theta_2>45$$

$$\left.\begin{aligned} C_w\phi_w &= C_w\phi_{\mathrm{SW}} \\ C_s\phi_s &= C_s\phi_{\mathrm{SW}} \end{aligned}\right\} \quad \theta_2=45 \tag{36}$$

where

$$A=\max\left\{\frac{45-\theta_2}{45},0\right\}$$

and

$$B=\min\left\{\frac{\theta_2}{45},\frac{90-\theta_2}{45}\right\}.$$

4.4. *Overview and discussion of influence coefficients*

The main points that arise from a close inspection of the influence coefficients, equations (11)–(36) are given below.

(1) The central-difference scheme influence coefficients become negative for $C_i>2D_i$, thus leading to oscillatory and non-convergent solutions. The cause of the negative coefficients is the use of downstream values in the flux approximations at high Peclet numbers.

(2) The upwind-difference scheme influence coefficients are unconditionally positive. This leads to physically reasonable solutions at all Peclet numbers. Its accuracy is, however, limited by its first-order discretization error. For flows aligned with the grids, and fairly fine grids, the scheme is accurate enough at high Peclet numbers. To reduce the discretization errors, the need arises to use finer grids which may prove expensive for practical applications.

(3) The hybrid-difference scheme influence coefficients are positive since they are just a combination of the central/upwind scheme. This practice ensures stability and improves accuracy of pure upwinding.

(4) The locally-exact-difference scheme influence coefficients are always positive and thus convergence and boundedness are assured. For one-dimensional steady-state flow, the scheme produces accurate solutions for any Peclet number, even for a fairly coarse grid.

(5) The power-difference scheme influence coefficients are just variations of the locally-exact-difference scheme, and the same comments apply.

(6) The quadratic upstream-difference scheme influence coefficients may suffer from instabilities, that is, the coefficients can become negative when con-

vection effects are large. Furthermore, negative coefficients appear when $(A_p - S_p) < 0$. A simple way to overcome this is to switch over to the upwind-difference scheme at a certain Peclet number. However, this treatment destroys generality, which for practical implementation, is a strong desideratum.

(7) The extended version of the quadratic upstream-difference scheme possesses positive influence coefficients, regardless of the magnitude of the convection term, but the source terms may still induce negative coefficients.

(8) The revised version of the quadratic upstream-difference scheme—extended ensures always positive coefficients, by introducing a linear source which depends on the previous iteration field values.

(9) The skew-difference scheme influence coefficients can be a mixture of both positive and negative terms. The grid point coefficients (i.e. $A_E$, $A_W$, $A_N$, $A_S$) can become negative because they include elements of outflows. However, the remaining coefficients (i.e. $A_{SW}$, $A_{SE}$, $A_{NW}$, $A_{NE}$) are positive and have some favourable stabilizing consequences.

(10) The residual-difference scheme, achieved by the inclusion of exponential functions, has similar coefficients to those of the central-difference scheme, except that the diffusion terms are appropriately modified.

(11) The novel UPSTREAM scheme presented here, and its variants [11], is a flow-oriented scheme with a difference in that it overcomes the problems of nonconvergence by formulating the influence coefficients so as to ensure positive values only. Here also false diffusion is considerably reduced or virtually eliminated [17].

It should be mentioned that a disadvantage of all 'skew schemes' is that 'conservation' of energy, species, etc. cannot be guaranteed. This is a serious defect, and a future development should be an additional 'correction' stage in the solution procedure, to reinstate conservation in case of its violation.

(12) In general, the boundary conditions for the test problem are incorporated by modifying the B-coefficients in the finite-domain equations. For the QUDS/E/R schemes, a problem occurred with the extra upstream values that are required. This was dispensed with by setting the upstream value either to the boundary value or the first internal grid-point value. It was found in other work, for two-dimensional laminar flow problems [23], that both treatments lead to similar results. For the other schemes no special treatment was required.

### 4.5. *The magnitude of 'false diffusion'*

The following are the most widely used approximate expressions for the magnitude of the 'false-diffusion' coefficient, as applied to two-dimensional problems that are simulated using the upwind scheme:

*Wolfshtein (1968)* [19]

$$\Gamma_{\text{false}} \cong 0.36\rho|\mathbf{V}|\Delta \sin 2\theta; \qquad (37)$$

*De Vahl Davis and Mallinson (1976)* [20]

$$\Gamma_{\text{false}} \cong \frac{1}{4(\sin^3\theta + \cos^3\theta)}\rho|\mathbf{V}|\Delta \sin 2\theta; \qquad (38)$$

*Leschziner (1980)* [21]

$$\Gamma_{\text{false}} \cong \frac{\sqrt{2}}{4}\rho \sin\left(\frac{\pi}{4} + \theta|\mathbf{V}|\Delta\right)\sin 2\theta \qquad (39)$$

where $\theta$ is the flow angle and $\Delta$ the (uniform) mesh size.

All of the above expressions yield $\Gamma_{\text{false}} = 0$ at $\theta = 0$, $\pi/2$ and a maximum value of $0.36\rho|\mathbf{V}|\Delta$ at $\theta = \pi/4$. This implies that at an angle of $\theta = 45°$, the upwind-difference scheme introduces a 'diffusion' coefficient equivalent to $|Pe| \simeq 2.8$, regardless of the magnitude of the real Peclet number.

The De Vahl Davis and Mallinson [20] approximation, equation (38), was used in this work to quantify the 'false diffusion'.

## 5. COMPUTATIONAL DETAILS

All the above schemes were implemented in a general purpose two-dimensional code which uses the SIMPLE algorithm of Patankar and Spalding within a finite-difference, control-volume formulation, described in detail in ref. [1]. The SIMPLE procedure leads to an iterative scheme which involves the repeated solution of sets of linear equations by a TDMA algorithm. The computer code itself is a variant of 2/E/FIX originally developed by Pun and Spalding [22].

The computational grid spanned 0.35 m radially with 11 grid positions and 0.47 m axially with 10 grid positions. The distribution of the grid lines was as follows:

$x$: 0.0, 0.03, 0.06, 0.10, 0.16, 0.22, 0.28, 0.34, 0.40, 0.47

$y$: 0.0, 0.015, 0.025, 0.045, 0.075, 0.105, 0.135, 0.175, 0.225, 0.275, 0.350.

The solution domain was chosen to enclose the jet expansion. In the calculations considered here, 100 iteration cycles were sufficient to converge results to 0.1% in pressure. The computer time for such a calculation was 180 s on a PRIME 750, for the UDS and 200 s on the same machine for the UPSTREAM scheme.

## 6. RESULTS AND DISCUSSION

The results obtained are presented in Figs. 4–23.

### 6.1. *The general flowfield*

Figures 4–23 present typical results from the standard calculation (e.g. with conditions as described in Section 2), obtained using the UDS and the standard turbulence model constants. The results are presented in the form of velocity vectors and contour plots.

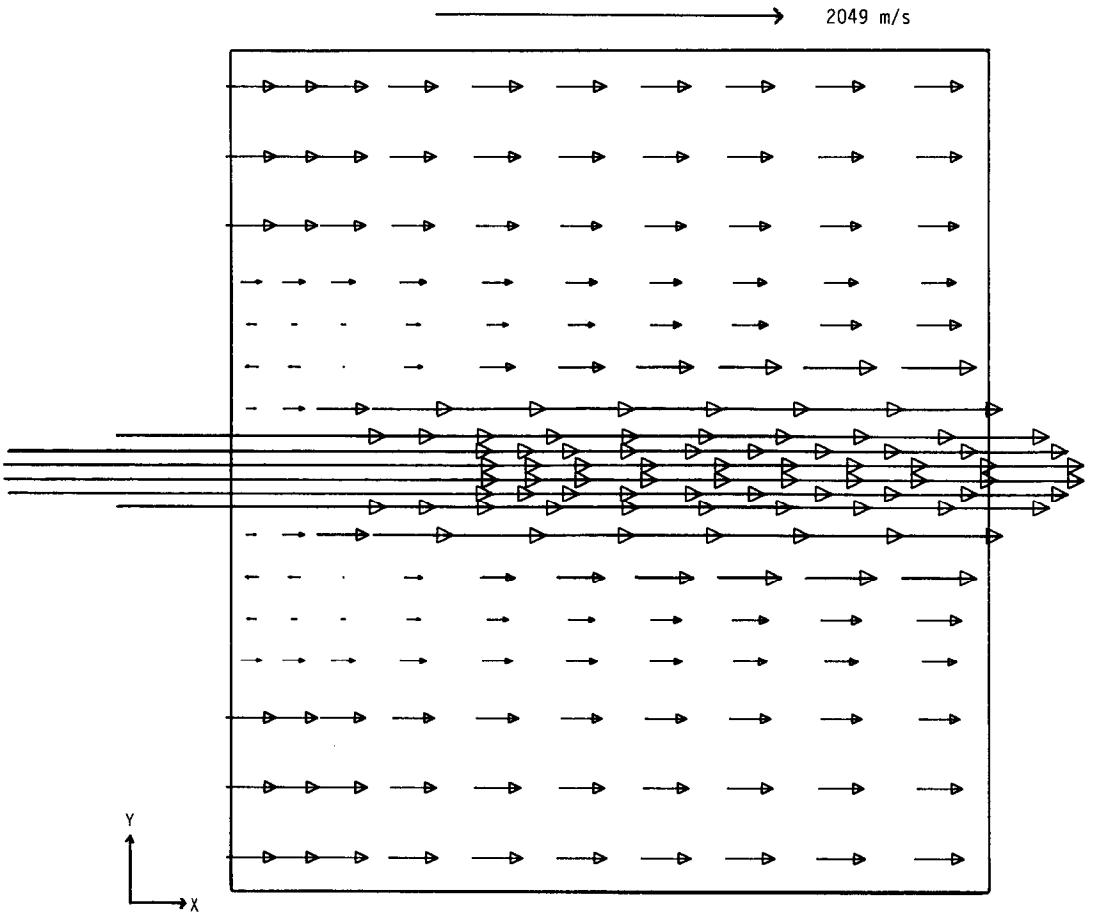


FIG. 4. Velocity vector plot (UDS).

Figure 4 presents the velocity vectors and Fig. 5, contour plots of the axial velocity component. There is clearly a recirculation region next to the wall with a minimum value of $u = -53.0$ m s$^{-1}$, extending to about 0.08 m downstream from the nozzle exit plane.

Figure 6 describes the temperature distribution in the form of isothermal contours for values between 216 and 1060 K in ten equal intervals. The temperatures near the wall are higher than those in the nozzle stream. This is a hydrodynamical feature of the flow discussed in detail in ref. [1]. Figure 7 presents contours of density in 15 equal intervals between 0.31 and 1.57 kg m$^{-3}$.

Pressure contours are displayed in Fig. 8. The pressures at the nozzle exit, the freestream and just downstream of the nozzle wall are 200, 100 and 81 kPa, respectively. The pressure is higher in the nozzle exit stream than in the freestream and the expansion of the nozzle flow is enhanced by the reduced pressure in the base region. As the nozzle flow expands downstream the pressure on the jet axis decreases to a minimum, 87 kPa, at a distance of 0.16 m from the nozzle-exit plane, and then increases again, as the expanding flow is reflected back to the plane axis, to a maximum of 115 kPa at a distance of 0.37 m. The pressure radial profile just downstream of the wall shows a small lowering of the pressure behind the nozzle wall, the gradient of which drives the recirculating flow; the differences between the ambient pressure and this reduced pressure may cause a significant drag force.

Figure 9 presents contours of kinetic energy of turbulence. The predicted minimum value is about $1.7 \times 10^{-4}$ kg m$^{-1}$ s$^{-1}$ and the maximum about 1.0 kg m$^{-1}$ s$^{-1}$ (i.e. between 10 and 6000 times the laminar value). The wall has a large effect on turbulence kinetic energy in the subsonic region, and the turbulence energy is substantial in the mixing layer and falls away rapidly on moving into the freestream. Figure 10 presents contours of effective viscosity.

### 6.2. *Predictions obtained by the various discretization schemes*

Figures 8–23 are devoted to comparing results obtained by using the various discretization schemes, described earlier. The presented comparisons are selected to display the greatest prediction differences among the schemes and refer to two downstream

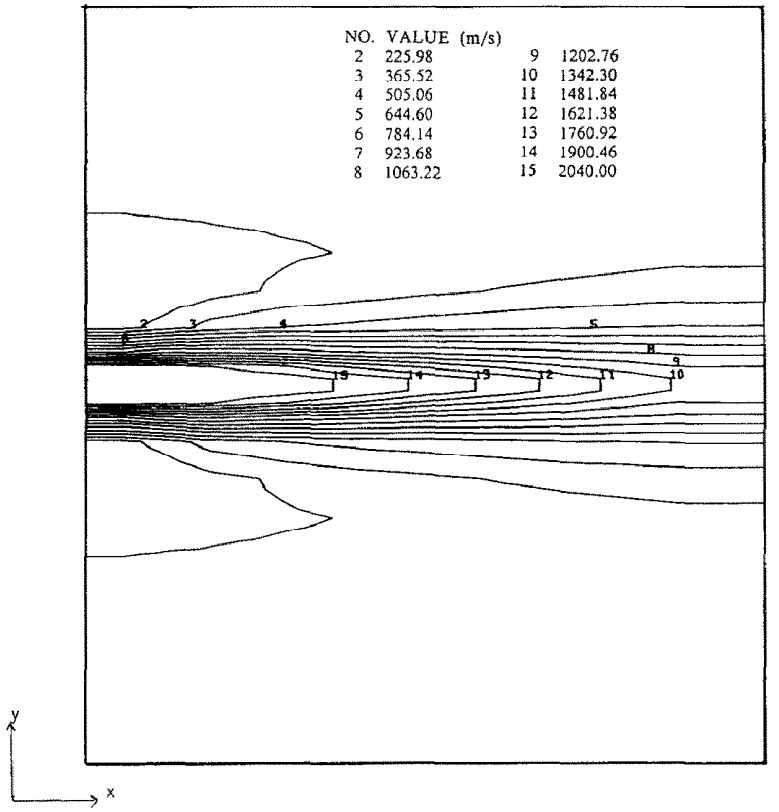


FIG. 5. Axial velocity contour plot (UDS).

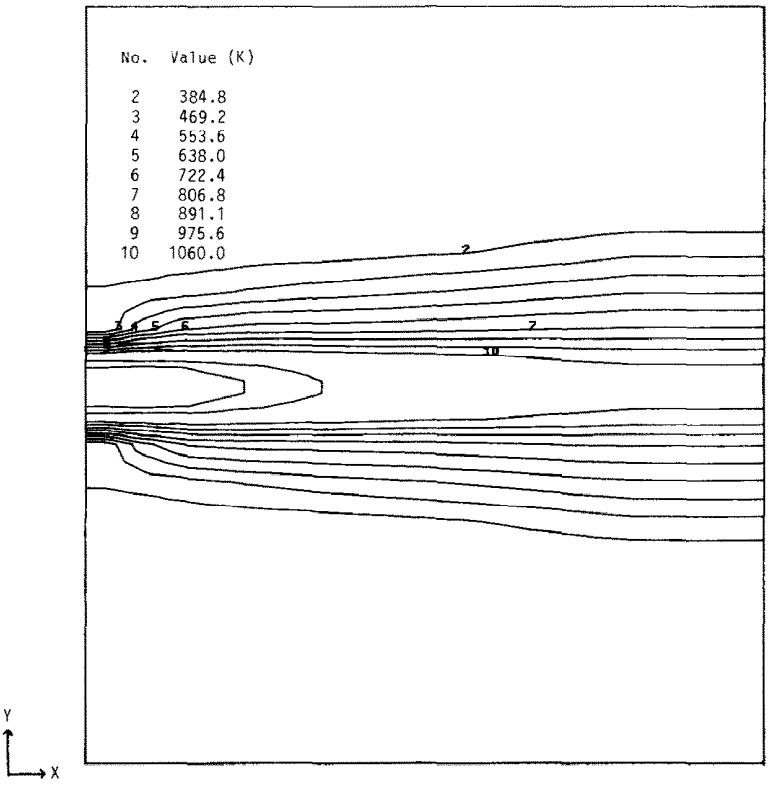


FIG. 6. Temperature contour plot (UDS).

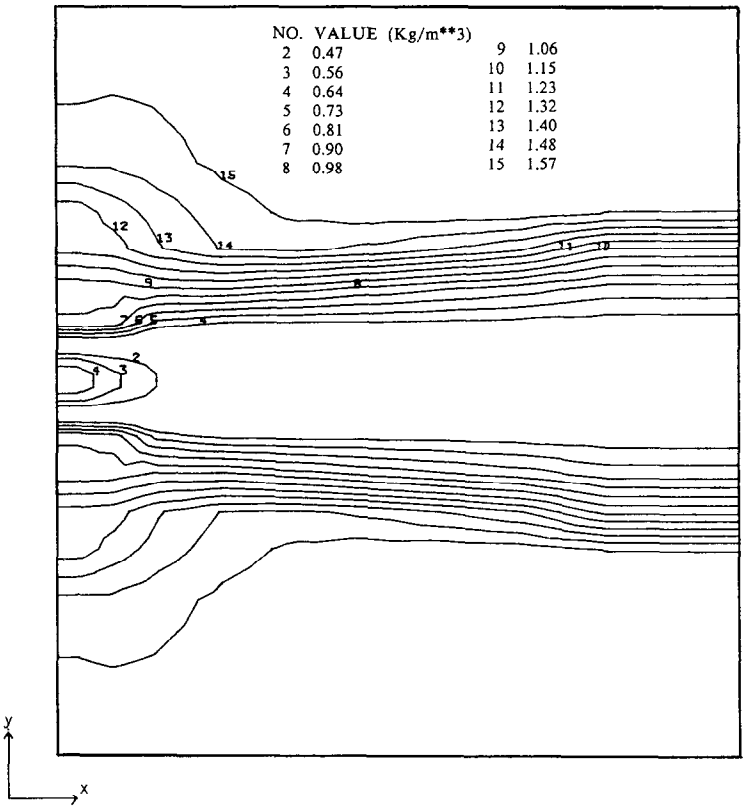


FIG. 7. Density contour plot (UDS).

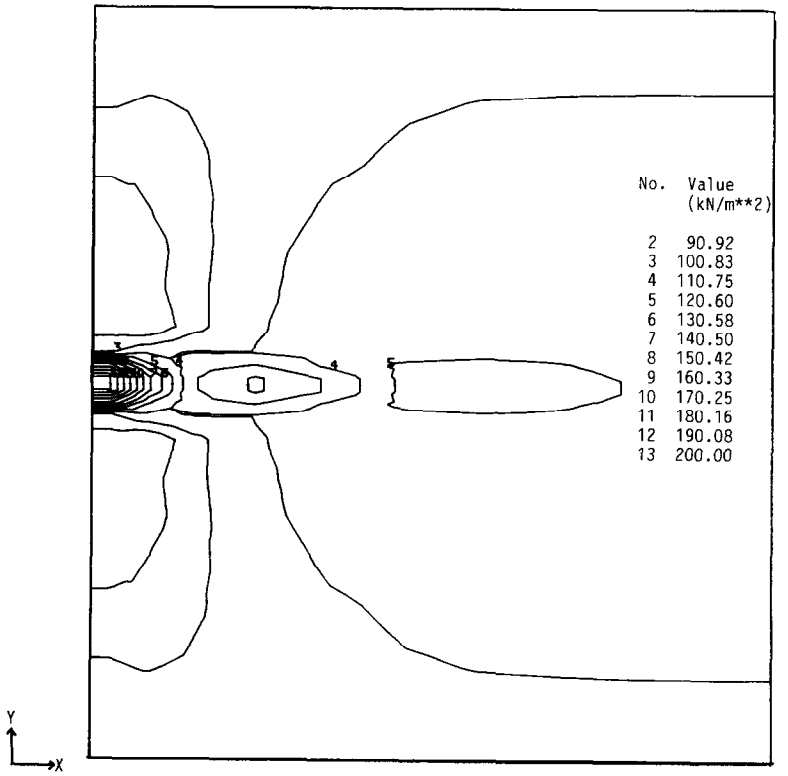


FIG. 8. Pressure contour plot (UDS).

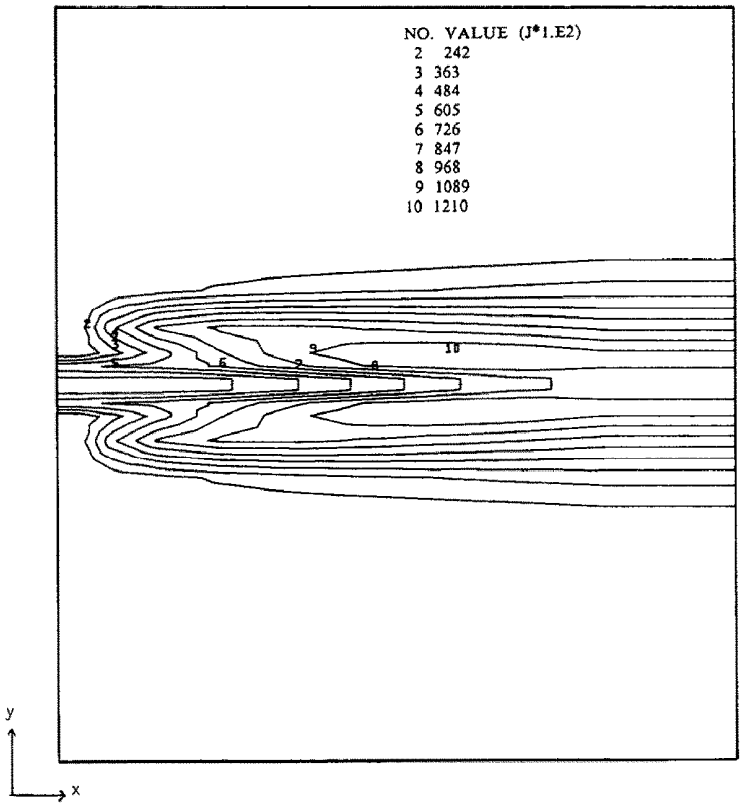


FIG. 9. Kinetic energy of turbulence contour plot (UDS).

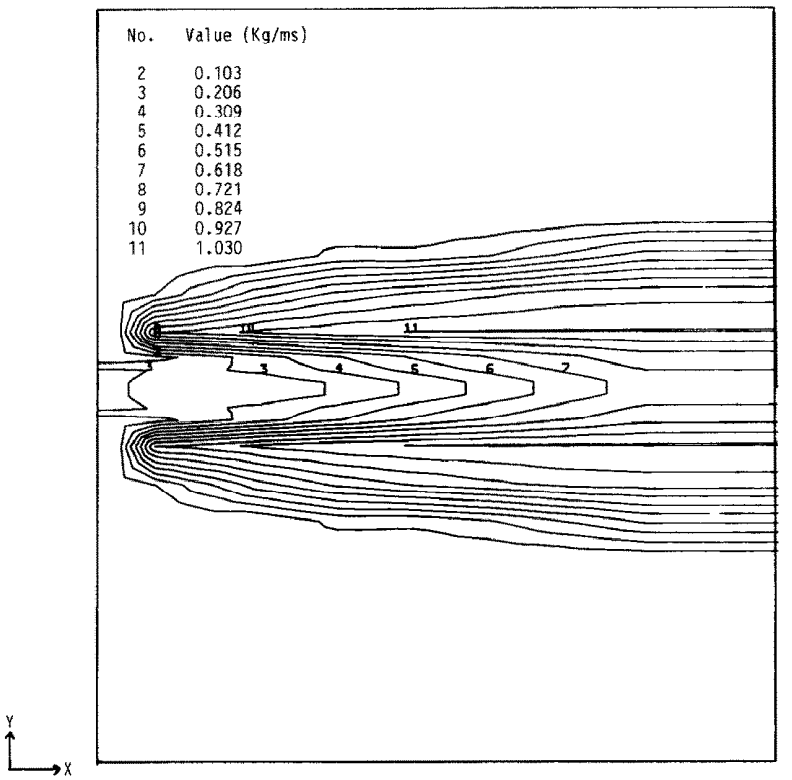


FIG. 10. Effective viscosity contour plot (UDS).

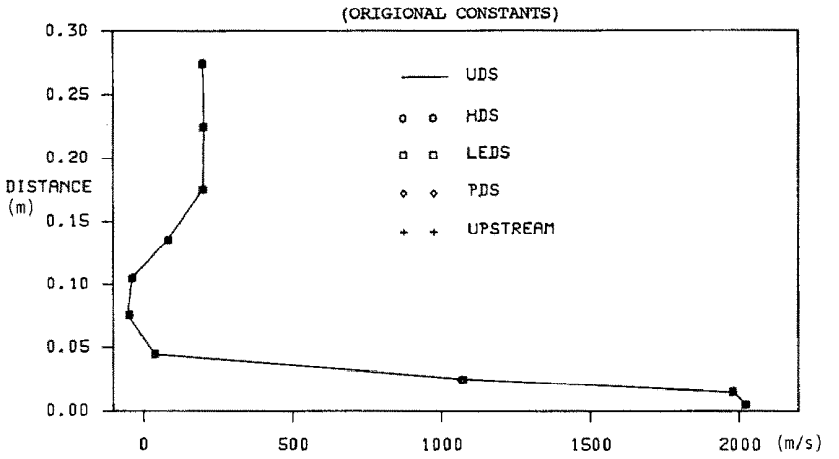


FIG. 11. Axial velocity profiles at IX = 2 station.

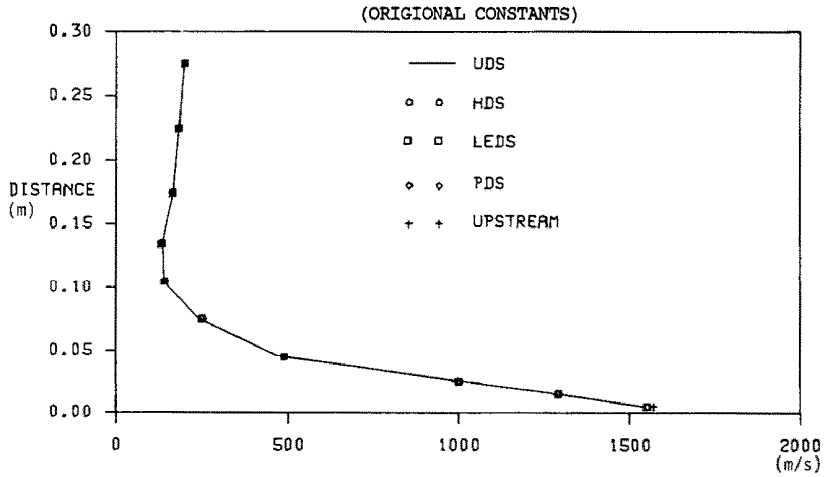


FIG. 12. Axial velocity profiles at IX = 8 station.

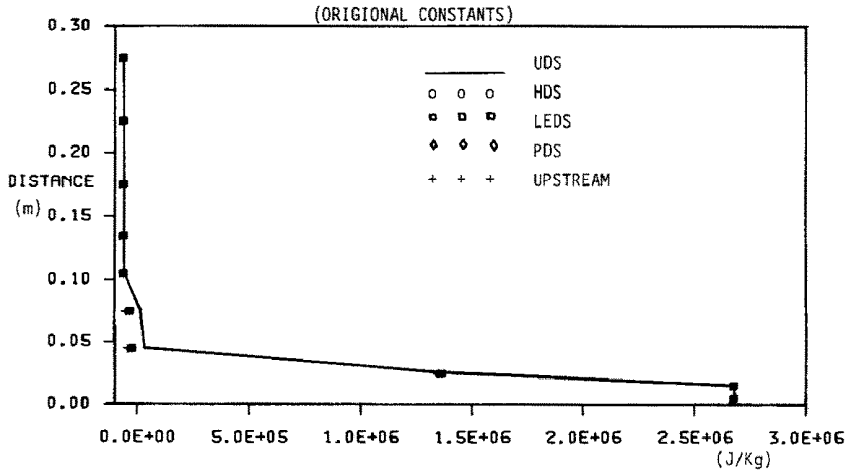


FIG. 13. Enthalpy profiles at IX = 2 station.

stations, identified by IX = 2 (at a distance of 0.03 m from the nozzle wall) and IX = 8 (at a distance of 0.34 m from the nozzle wall).

From the eleven schemes used only five led to converged solutions. They are the UDS, HDS, LEDS, PDS and the UPSTREAM schemes. The rest failed to converge for this test case despite the authors' considerable efforts with various combinations of relaxation parameters and procedures. It has been observed elsewhere [23], that as the grid Peclet number rises so several of the 'higher order' schemes become increasingly unstable and eventually fail. As such, it is not so surprising that the higher order schemes failed to converge on the present problem, since the grid Peclet number is high at various locations within the integration domain. Figures 11 and 12 present axial velocity profiles at IX = 2 and 8, respectively.

Comparison of predictions for the axial velocity, $u$, reveals that all five schemes lead to virtually identical predictions throughout the field. The maximum discrepancies occur at IX = 8, again very near the axis, where the UDS predicts slightly lower velocity values than the rest.

Figures 13 and 14 present enthalpy profiles at IX = 2 and 8, respectively, as predicted by the five schemes that led to converged solutions. At IX = 2 the predictions with all schemes are virtually the same except in the recirculation region where all other schemes predict a marginally sharper profile than the UDS. At IX = 8 the maximum discrepancies occur near the axis. There, the UDS underpredicts the enthalpy value compared with the other schemes, and particularly with respect to the UPSTREAM prediction (a difference of around 10%).

### 6.3. *Turbulence model uncertainties*

To allow for some quantification of the discrepancies found among the various scheme predictions, compared with the uncertainties in modelling, e.g. turbulence, a change was effected in one of the turbulence-model constants. Thus, $C_\mu$ was changed from 0.09 to 0.07 and the runs were repeated. A summary of the results obtained is presented in Figs. 14–22.

Figures 15–18 correspond to Figs. 11–14 and show the predictions for axial velocity and enthalpy at IX = 2 and 8 with the modified constants. Figure 18 displays the predictions for the enthalpy radial distribution at IX = 8, as obtained by the five schemes that led to converged solutions, with the modified turbulence-model constant. Comparing these results with Fig. 14 (case with the original constant) we observe that the maximum discrepancy between the UPSTREAM and the rest of the schemes is now somewhat more pronounced at radial distances of 0.05–0.10 m. Figures 19–22 present the profiles for modified/unmodified constants with one other scheme, i.e. LEDS or UPSTREAM. For a more direct comparison Figs. 20 and 22 present the IX = 8 velocity and enthalpy profiles predicted by the UDS for $C_\mu = 0.09$ and 0.07 and also the profiles predicted by the scheme that led to the largest discrepancy, namely UPSTREAM, when used with $C_\mu = 0.09$. It is seen that at IX = 8 the discrepancies due to the different $C_\mu$ values are significantly larger than those due to the scheme used. At IX = 2, Figs. 19 and 21, the discrepancies due to the turbulence-model constant are of the same magnitude as the discrepancies due to the schemes, for both the velocity and the enthalpy. False-diffusion errors are then not significant in the high-shear, high-velocity cases considered here, at least when compared to the uncertainties introduced by the turbulence models.

### 6.4. *False-diffusion levels*

Equation (38) above, was used to quantify the magnitude of 'false diffusion'. A map of false-diffusion values, in the form of a contour plot is given in Fig. 23. The contours present values of the ratio of the 'false-diffusion' coefficient over the laminar viscosity.

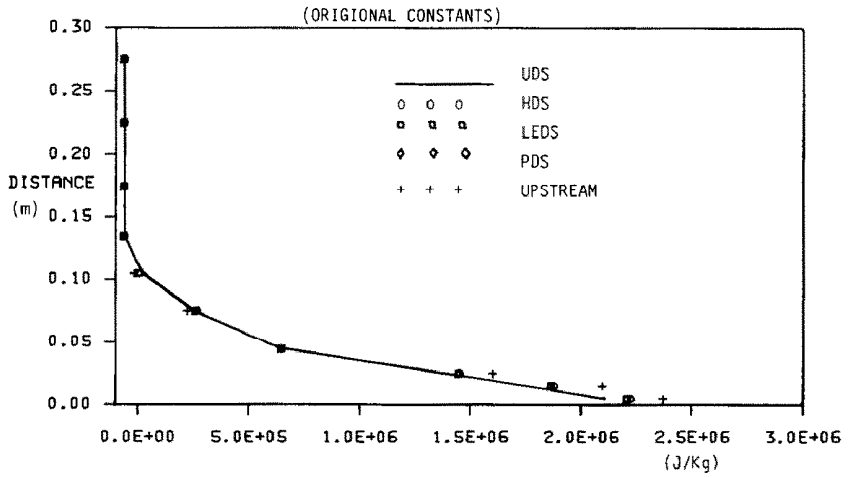


FIG. 14. Enthalpy profiles at IX = 8 station.

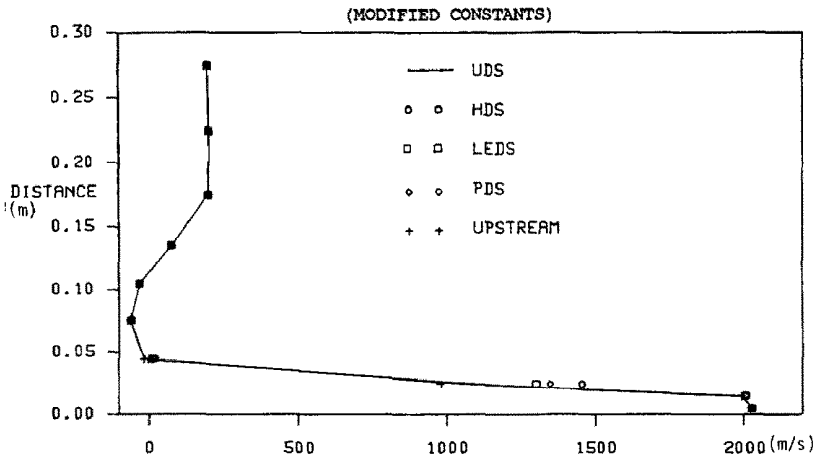


FIG. 15. Axial velocity profiles at IX = 2 station.

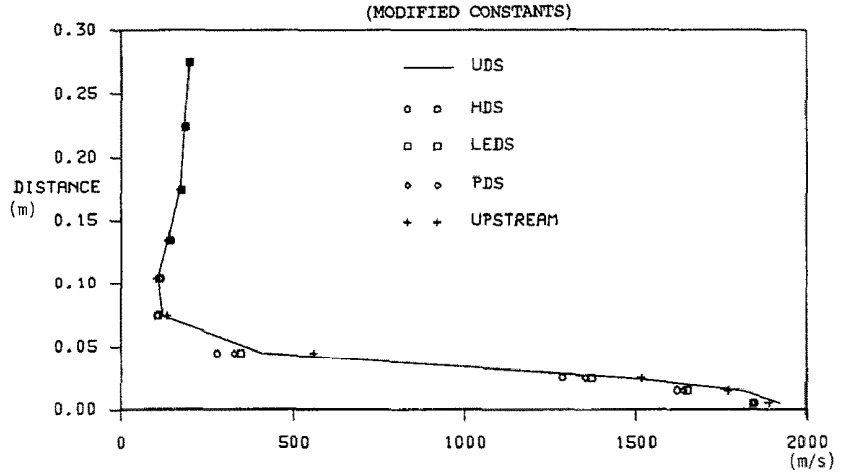


FIG. 16. Axial velocity profiles at IX = 8 station.

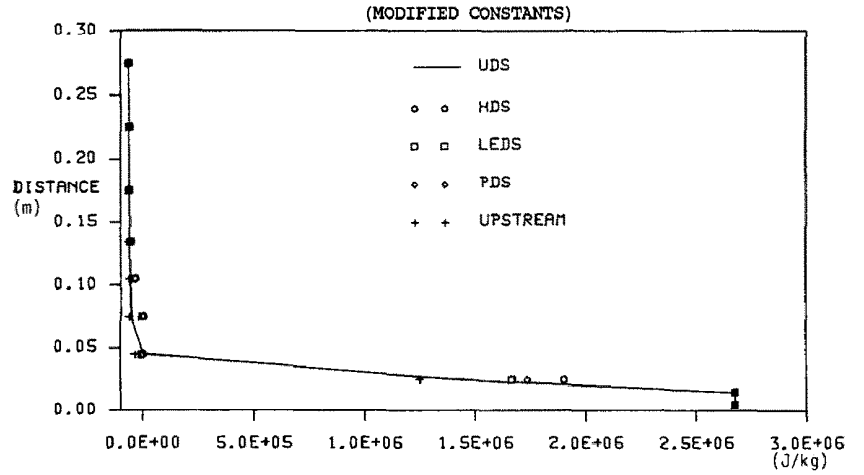


FIG. 17. Enthalpy profiles at IX = 2 station.

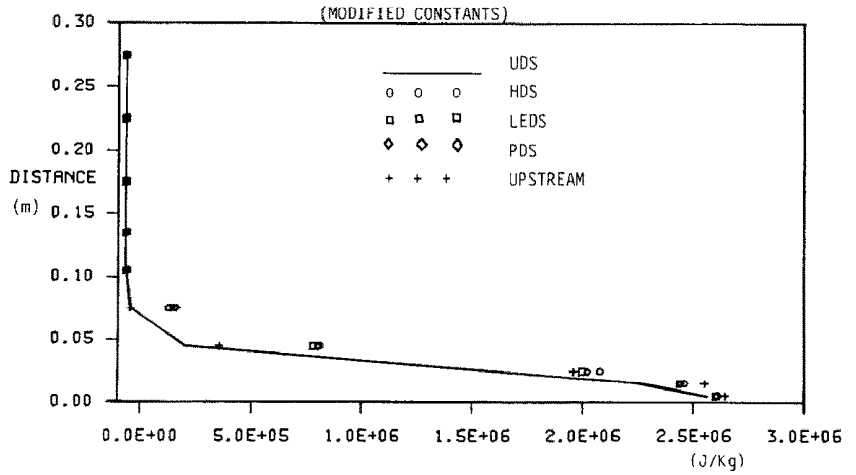


FIG. 18. Enthalpy profiles at IX = 8 station.

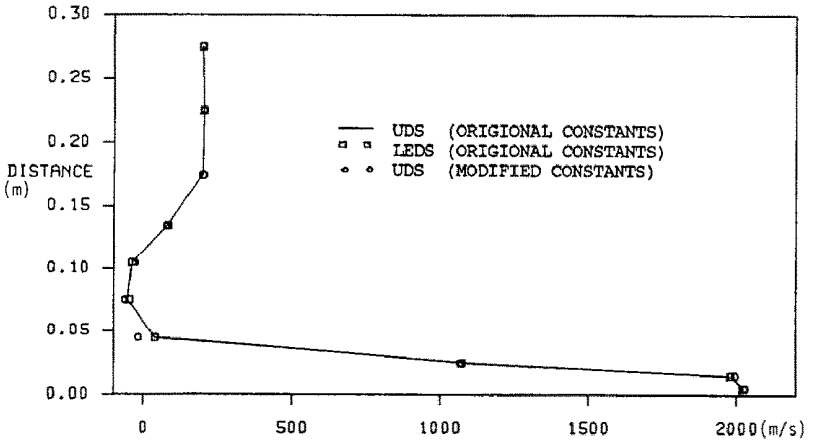


FIG. 19. Axial velocity profiles at IX = 2 station.

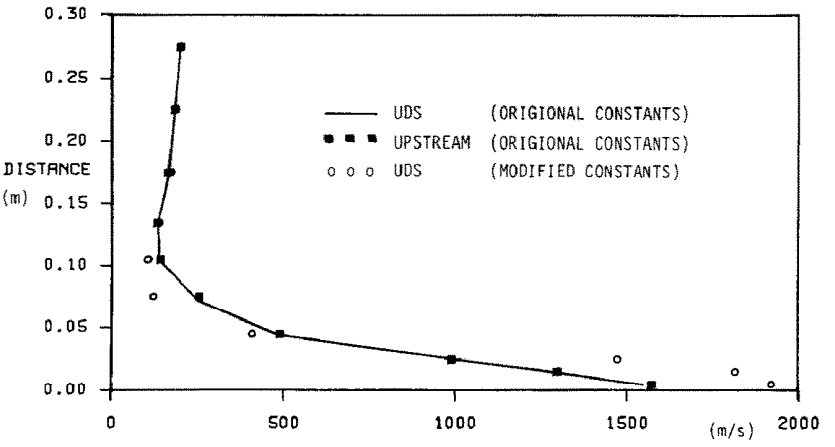


FIG. 20. Axial velocity profiles at IX = 8 station.

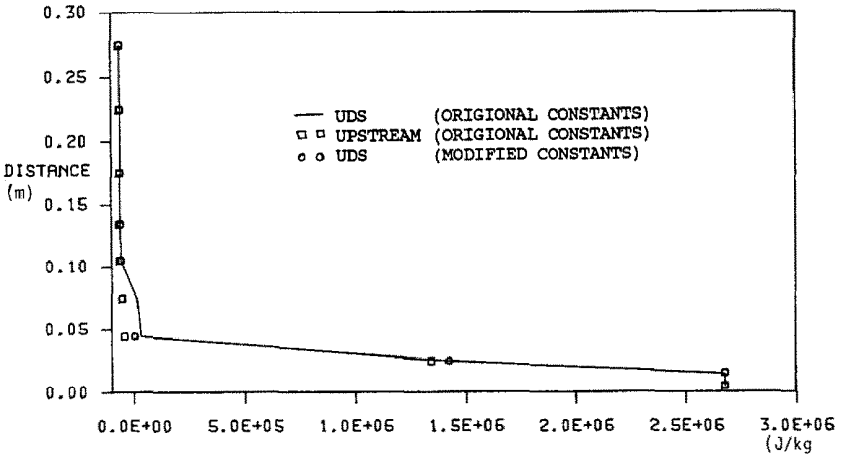


FIG. 21. Enthalpy profiles at IX = 2 station.

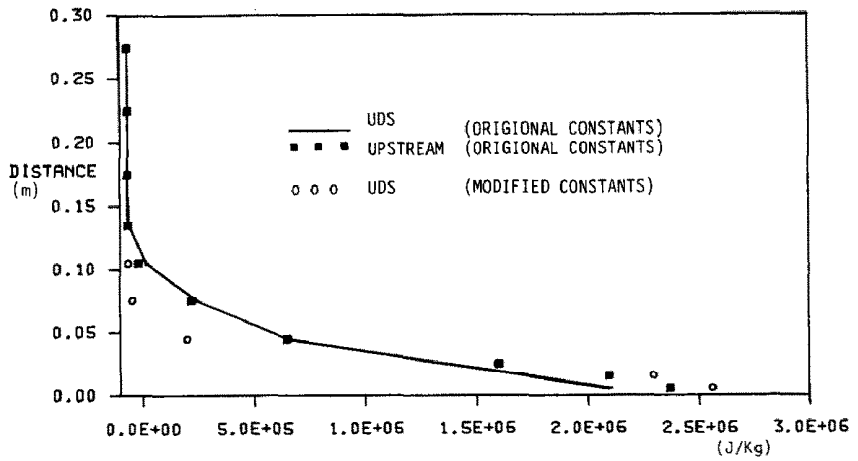


FIG. 22. Enthalpy profiles at IX = 8 station.

It is seen that the magnitude of false diffusion, as predicted by equation (38), is at most 15 times greater than the laminar viscosity. The turbulence viscosity is between 10 and 6000 times the laminar value, so, at worst, the false diffusion is 1.5 times the real diffusion, that proves insignificant as far as predictions in these highly convective flows are concerned.

## 7. CONCLUSIONS

A comparative study has been performed on the behaviour of eleven numerical schemes for convection, as applied to simulations of supersonic-jet flow and heat-transfer problems.

The higher-order schemes based on quadratic upstream differencing, and Raithby's skew scheme unfortunately failed to converge for the problems considered in this study, despite the authors' best efforts, that included heavy relaxation and Peclet-number-based switches. This behaviour is consistent with the unstable nature of those schemes in applications to general practical cases. The UPSTREAM skew scheme led successfully to converged solutions, requiring about 10% more CPU time than the UDS, to obtain the same degree of convergence. The schemes that converged (e.g. UDS, HDS, LEDS, PDS and UPSTREAM), led to velocity and temperature results that were only marginally different. The maximum differences occurred near the jet axis at a distance of 0.34 m from the base wall, and were consistently less than 10% (the maximum being the difference in enthalpy predictions between the UPSTREAM and the upwind schemes). Indeed, the observed differences were consistently less than the differences introduced by changing one of the turbulence-model constants.

It is concluded that for the high-shear, high-velocity problems encountered here, even in the presence of recirculation, the UDS scheme is probably the best choice, differing only marginally in accuracy from the schemes that departed most, namely the LEDS and the UPSTREAM. It is stable, simple to understand

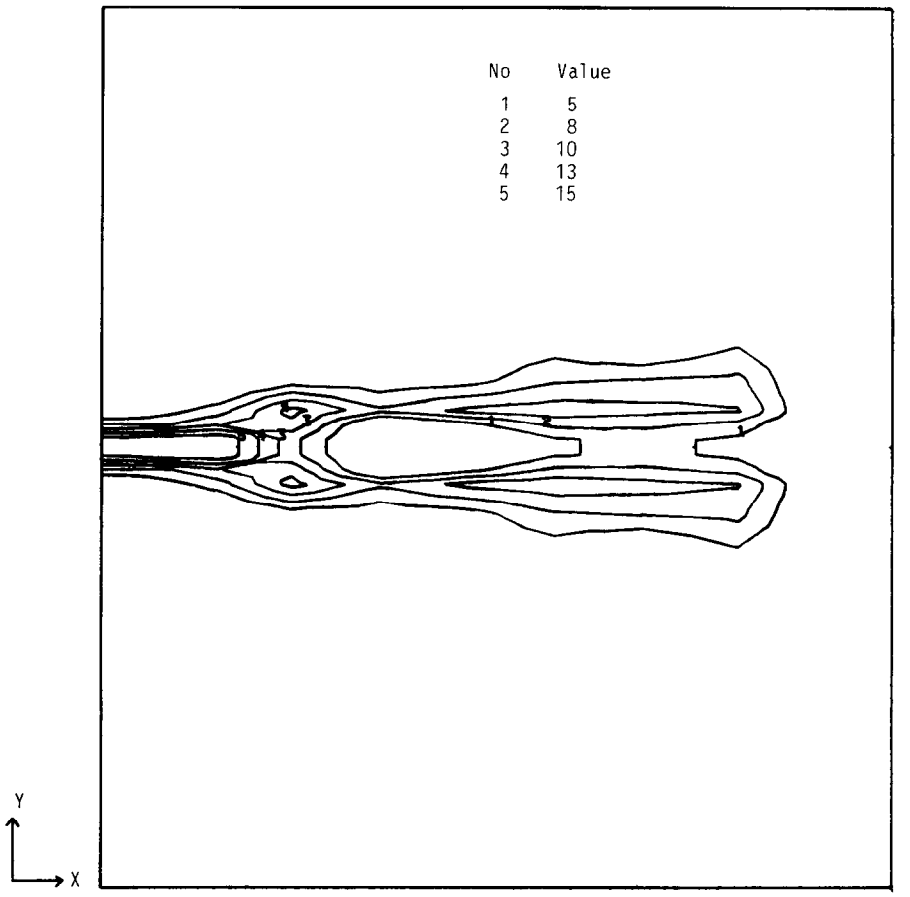


FIG. 23. False-diffusion/real-diffusion contour plot (UDS).

and implement. It is also pointed out that in general applications care must be taken to sort out discrepancies that arise separately from mathematical modelling, such as turbulence modelling, and from numerical schemes. Therefore, for flows of practical interest, turbulence-modelling research should be coupled with research directed towards developing more accurate numerical prediction schemes.

Finally, while numerical and physical-reasoning analyses increase confidence in prediction techniques, nothing surpasses good, high resolution measured data which is, regrettably, currently not available for the flows studied here.

## REFERENCES

1. A. C. H. Mace, N. C. Markatos, D. B. Spalding and D. G. Tatchell, Analysis of combustion in recirculating flow for rocket exhausts in supersonic streams, AIAA, 81-1386R, *J. Spacecraft Rockets* **19**(6), 557–563 (1982).
2. A. C. H. Mace, Unpublished work.
3. S. V. Patankar, *Numerical Heat Transfer and Fluid Flow*. McGraw-Hill, New York (1980).
4. G. J. C. De Allen and R. V. Southwell, Relaxation methods applied to determine the motion in two dimensional of a viscous fluid past a fixed cylinder, *A. J. Mech. Appl. Math.* **VIII**(2), 129 (1955).
5. R. Courant, E. Isaacson and M. Rees, On the solution of nonlinear hyperbolic differential equations by finite-differences, *Commun. Pure Appl. Math.* **5**, 245 (1952).
6. D. B. Spalding, A novel finite-difference formulation for differential expressions involving both first and second derivatives, *Int. J. Numer. Meth. Engng* **4**, 557–559 (1972).
7. D. N. Allan and R. V. Southwell, The motion, in two dimensions, of a viscous fluid past a fixed cylinder, *Q. J. Mech. Appl. Math.* **8**, 2 (1955).
8. B. P. Leonard, A stable and accurate convective modelling procedure based on quadratic upstream interpolation, *Comp. Meth. Appl. Mech. Engng* **19**, 59–98 (1979).
9. A. Pollard and A. L. W. Siu, The calculation of some laminar flows using various discretization schemes, *Comp. Meth. Appl. Mech. Engng* **35**, 293–313 (1982).
10. G. D. Raithby, A critical evaluation of upstream differencing applied to problems involving fluid-flow, *Comp. Meth. Appl. Mech. Engng* **9**, 79–103 (1976).
11. G. D. Raithby, Skew upstream differencing schemes for problems involving fluid-flow, *Comp. Meth. Appl. Mech. Engng* **9**, 153–164 (1976).
12. R. F. Le Feuvre, The application of a semi-orthogonal finite integral technique to predict inclined-plane and cylindrical Couette flows, Rep. No. EF/TN/A/33, Imperial College, London, and Rep. No. HTS/74/5, Imperial College, London (1970).
13. I. Zuber, A mathematical model of the combustion chamber, Bechovice Monographs and Memoranda, No. 12 (1972).

14. J. N. Lillington, A vector upstream differencing scheme for problems in fluid-flow involving significant source terms in steady state linear systems, *Int. J. Numer. Meth. Fluids* **1**, 3–16 (1981).
15. M. K. Patel, Full formulation of the skew scheme, NUMOD Report No. 85/3, Thames Polytechnic, London (1985).
16. T. K. Bhattacharyya and A. B. Datta, A residual method of finite differencing for elliptic transport problem and its applications to cavity flow, *Int. J. Numer. Meth. Fluids* **5**, 71–80 (1985).
17. M. K. Patel, N. C. Markatos and M. Cross, Method of reducing false-diffusion errors in convection–diffusion problems, *Appl. Math. Modelling* **9**, 302–306 (1985).
18. S. V. Patankar and D. B. Spalding, A calculation procedure for heat, mass and momentum transfer in parabolic flows, *Int. J. Heat Mass Transfer* **15**, 1787 (1972).
19. M. Wolfshtein, Numerical smearing in one-sided difference approximation to the equations of non-viscous flow, Report No. ET/TN/3, Mech. Engng Dept, Imperial College, London (1968).
20. De Vahl Davis and G. Mallinson, An evaluation of upwind and central difference approximations by study of recirculating flows, *Comput. Fluids* **4**, 29 (1976).
21. M. A. Leschziner, Practical evaluation of three finite-difference schemes for the computation of steady-state recirculating flows, *Comp. Meth. Appl. Mech. Engng* **23**, 293–312 (1980).
22. W. M. Pun and D. B. Spalding, A general computer program for two dimensional elliptic flows, Report No. HTS/76/2, Imperial College, London (1976).
23. M. K. Patel and N. C. Markatos, An evaluation of eight discretisation schemes for two-dimensional convection–diffusion equations, *Int. J. Numer. Meth. Fluids* **6**, 129 (1986).

## EVALUATION DE ONZE SCHEMAS DE DISCRETISATION POUR PREDIRE UN ECOULEMENT ELLIPTIQUE ET LE TRANSFERT THERMIQUE DANS DES JETS SUPERSONIQUES

**Résumé**—On décrit des études pour évaluer les erreurs numériques causées par une "fausse diffusion" et pour comparer les performances de schémas numériques décrivant la convection thermique elliptique dans des jets supersoniques ou subsoniques. Onze schémas sont considérés, mais des solutions convergentes ne sont obtenues qu'avec seulement cinq d'entre eux. Les résultats obtenus sont présentés et discutés. On conclut que pour les forts cisaillements et les écoulements à grande vitesse, le meilleur choix est probablement "upwind", malgré sa nature dissipative et les erreurs numériques associées à son utilisation ne sont pas plus significatives que celles introduites par les incertitudes des modèles de turbulence .

## UNTERSUCHUNG VON 11 DISKRETISIERUNGSVERFAHREN ZUR BESCHREIBUNG DER ELLIPITISCHEN STRÖMUNG UND DES WÄRMETRANSPORTS IN ÜBERSCHALL-STRAHLEN

**Zusammenfassung**—Der Bericht beschreibt Studien, in denen die numerischen Fehler bestimmt wurden, welche durch "falsche Diffusion" verursacht werden. Ein Vergleich der Leistungsfähigkeit von alternativen numerischen Verfahren wurde durchgeführt; die Verfahren beschreiben die elliptische Konvektionsströmung und den Wärmetransport beim Eintauchen eines Überschall-Strahls in eine Über- oder Unterschall-Strömung. Die Ergebnisse werden dargestellt und diskutiert. Elf Verfahren wurden in dieser Studie betrachtet—nur bei fünf von ihnen wurde eine Konvergenz der Lösungen beobachtet. Die Ergebnisse der funktionstüchtigen Verfahren werden dargestellt und diskutiert. Man folgert, daß für die betrachteten stark scherbeanspruchten Hochgeschwindigkeitsströmungen das "upwind"-Differenzenverfahren die beste Wahl darstellt, trotz seiner dissipativen Natur und der Tatsache, daß die numerischen Fehler nicht gravierender sind als jene, die durch Unsicherheiten im Turbulenz-Modell zustande kommen.

## ОПРЕДЕЛЕНИЕ ОДИННАДЦАТИ СХЕМ ДИСКРЕТИЗАЦИИ ДЛЯ РАСЧЕТА ЭЛЛИПТИЧЕСКОЙ МОДЕЛИ ТЕЧЕНИЯ И ТЕПЛООБМЕНА СВЕРХЗВУКОВЫХ СТРУЙ

**Аннотация**—Определены количественные оценки численных ошибок, вызванных «ложной диффузией»; сравнены эффективности альтернативных численных схем для описания модели эллиптического конвективного переноса импульса и тепла при смешении сверхзвуковых струй в сверх- и дозвуковых течениях Обсуждаются и анализируются результаты этих исследований. Рассматриваются также одиннадцать схем, но решения с хорошей сходимостью получены только для пяти из них. Приводятся и обсуждаются результаты, полученные с помощью наиболее удачных схем. Сделан вывод, что для высокоскоростных течений с большим поперечным градиентом скорости наиболее удачна разностная схема «противотока», несмотря на диссипативный характер, а также что численные ошибки, связанные с ее применением, не более существенны, чем ошибки, вводимые погрешностями турбулентных моделей.